Archives of Current Research International

Volume 24, Issue 5, Page 213-240, 2024; Article no.ACRI.116101
ISSN: 2454-7077

Analyzing the Impact of Wing Flexural Axis Position on the Dynamics of a Very Flexible Airplane Using Strain-based Formulation

Marcelo Santiago de Sousa [a*]
Flávio Luiz Cardoso Ribeiro [b],
Roberto Gil Annes da Silva [b], Pedro Paglione [b]
and Sebastião Simões da Cunha Junior [a]

[a] Federal University of Itajubá (UNIFEI), Av. BPS, 1303, Itajubá, MG, Brazil.
[b] Technological Institute of Aeronautics (ITA), Praça Marechal Eduardo Gomes, 50, São José dos Campos, SP, Brazil.

Authors' contributions

This work was carried out in collaboration among all authors. All authors read and approved the final manuscript.

Article Information

DOI: 10.9734/ACRI/2024/v24i5697

Open Peer Review History:
This journal follows the Advanced Open Peer Review policy. Identity of the Reviewers, Editor(s) and additional Reviewers, peer review comments, different versions of the manuscript, comments of the editors, etc are available here: https://www.sdiarticle5.com/review-history/116101

Received: 24/02/2024
Accepted: 26/04/2024
Published: 02/05/2024

Review Article

ABSTRACT

New technologies and the needs of specific missions have allowed and stimulated the development of airplanes with great structural flexibility. In these vehicles, there is a significant coupling between aeroelastic phenomena and flight dynamics. This has been a topic of research in recent years. Different methodologies have been studied to model the complete dynamics of flexible aircraft. One of these is the NFNS_s methodology (Non linear flight dynamics, non linear structural dynamics,

---

**Corresponding author: Email: marcelo.santiago@unifei.edu.br;*

strain based formulation). This article presents the use of this methodology in the analysis of the aeroelastic response and flight dynamics of a transport category aircraft with high structural flexibility. The effects of the wing elastic axis and the flexural axis positions were analyzed. Trimming, calculus of eigenvalues and time-marching simulations were carried out and the results were analyzed in detail. Some results were compared with those published in the literature. Similar trends were observed. This served as a qualitative validation of the methodology used. Some limitations of the study are described. The contributions of this work lie in the use of the NFNS_s methodology to analyze the effects of the elastic and flexural axis positions. In addition, the results of time marching simulations of the airplane modeled and the analysis carried out in great detail are other important novelty.

Keywords: Aeroelasticity; elastic axis; flexible airplane; flight dynamics; strain based formulation; flexural axis.

1. INTRODUCTION

Aircraft flight mechanics is commonly studied by different disciplines, including stability and control (flight dynamics) and aeroelasticity [1]. The former generally assumes the aircraft structure to be rigid and is focused on analyses of aircraft stability, controllability and handling qualities. The latter assumes a flexible structure and is focused on aeroelastic stability as well as analyses of aeroelastic response to external and internal perturbations. Traditionally, the frequencies of rigid body modes and flexible modes were quite distant, which allowed for separate analyses of flight dynamics and aeroelasticity. In recent years, this situation has changed.

New aircraft with lower structural weight are being developed. Consequently, these new aircraft have a higher structural flexibility [2], with a decreased frequency of the first flexible modes. As a result, this frequency may approach some rigid body mode frequencies which may result in a coupling between flight dynamics and aeroelastic response [3,4].

Aircraft are being developed for the mission of remote sensing. One of the requirements of such missions is long endurance. Consequently, design trends for these aircraft have pointed towards high aspect ratios, which in turn tend to increase their structural flexibility [5].

Another trend that has to be considered is the increasing deployment of unmanned aircraft. Since these aircraft are unmanned, they can be flown under higher load factors than those acceptable for manned aircraft. Higher load factors lead to large structural deformations and thus also contribute to an increased coupling between flight dynamics and aeroelastic response [3].

In view of the above mentioned design trends, it became necessary to develop mathematical models that incorporate and integrate the disciplines of flight dynamics and aeroelasticity in order to account for the coupling between them. Different modeling methodologies have been developed, including those described in [6,7,8,9,3,10,11]. These modeling methodologies are generically named NFLS (Non Linear Flight Dynamics – Linear Structural Dynamics) in [12]. This methodology uses the nonlinear rigid body flight dynamics coupled with linear structural dynamics. Tuzcu and Meirovitch [13,14] developed one different methodology in which the structural dynamics is also linear. Although these methods can be used in most situations, it is not sufficient for a complete analysis when there are large structural deformations [15]. Alternative methodologies are being used in order to consider large deformations [16,17,15,18,5,12-20,21]. These references use beam formulation in order to capture geometrically non linear structural deformations [20].

There are three ways to implement beam formulation: displacement formulation (d-beams) [4], strain formulation (s-beams) [16,22,5,19-20] or the intrinsic formulation (i-beams), [15]. Their difference lies in the independent variables chosen to represent the displacement field and in the treatment of the beam reference’s line rotation [20].

The authors have used the strain based formulation in their research. In first publications related to this formulation, shear strains were not considered, but the formulation was expanded in order to consider also shear strains [17,15].

The methodology in which nonlinear structural dynamics are modeled with strain based formulation is generically named here as

NFNS_s (Non Linear Flight Dynamics – Non-linear Structural Dynamics, strain based formulation) [12]. NFNS_s has being continually developed by Cesnik and his co-workers and is described in details in Brown [16], Ribeiro [18], Shearer [5], and Su [19,20]. The NFNS_s formulation considers large deformations and inertial coupling between elastic and generalized coordinates [12].

Once the equations of motion are defined, data of flexible airplane are needed in order to run simulation, and to analyze the results obtained.

The acquisition of flexible airplane data is not an easy task. Due to this fact, Da Silva used the NFLS methodology to implement the mathematical model of one conceptual flexible airplane representative of medium size jet airplanes like Embraer EMB-190/195 and Boeing 737-200/300 [6].

Sousa modeled the same conceptual airplane with the NFNS_s methodology. This model was used to make comparisons between the NFLS and NFNS_s methodologies and to implement robust nonlinear flight control laws [12].

Once having the airplane data and the equations of motion modeled, some simulations can be performed in order to analyze the couplings between flight and aeroelastic dynamics. The knowledge of the couplings contributes to the design and development of flexible airplanes.

After research in literature it was found some references that explore the effects of structural stiffness [6, 23,24,18,12-19] and of the elastic axis [25,26] on aeroelasticity and flight dynamics of flexible airplanes.

The aeroelasticity discipline has as goal guaranteeing the non-occurrence of either flutter or divergence in the operational airplane airspeeds. One classical flutter mechanism known in english literature is the bending-torsion coupling [27]. One way known to decrease this coupling is using the flexural (elastic) and mass axes coincident. Even in this case, flutter can still be present if the non-stationary damping terms are considered [27]. Despite that, the proper location of the elastic axis in relation to the mass axis continues to be one form to delay the occurrence of flutter.

Babcock [28] used the software ASWING developed by Drela [29] to model and evaluate the flight dynamics coupled with the aeroelastic response of one micro aerial vehicle (MAV). Babcock evaluated the effect of wing elastic response on flight and on aeroelastic dynamics.

These recent researches have shown the importance in analyzing not only the structural stiffness, but also the elastic axis position during the design and development of flexible airplanes, but, for the author´s knowledge, until today the NFNS_s methodology was not used to evaluate the effects of elastic axis/ flexural axis positions in one very flexible transport category aircraft, and this is the main contribution of this work. Other contribution is the use of time marching simulations to verify the occurrence of flutter (in time domain), beyond the common technique of finding the eigenvalue solution of aeroelastic equations. One physical interpretation is given to the results presented here.

Although this paper and some references describe the effects of the elastic axis position, the own definition of this parameter can cause controversies. Stodieck, Cooper, Weaver [30] describe the correct definition for the elastic axis positions and for the local and global flexural axis. For convenience, these definitions will be repeated here also:

a) The shear center is the position on a two-dimensional cross-section where there is zero rate of twist along the beam for a shear load applied to that cross-section and does not include bend/ twist coupling.

b) The elastic axis is the locus of the shear center along the wing. Note here, that, according to the authors understanding, the shear load applied to one cross-section will affect not only the cross-section where the load was applied, but also the other cross-sections, along the wing.

c) The reference axis is the locus of some geometric or otherwise characteristic position. In this work, the reference axis was located in one fixed position, described in Sousa [12], Sousa, et.al [31].

d) The flexural center is the position of a shear load on a streamwise wing cross-section relative to the wing root, where there is zero twist relative to the wing root, but not necessarily elsewhere on the wing.

e) The local flexural axis is the locus of all flexural centers along the wing.

f) The global flexural axis is the position of a distributed set of loads applied simultaneously on the wing, that will produce zero twist along the wing.

According to the definitions presented, it seems the local and global flexural axes can have much more importance. For this reason, the local and global flexural axis were also considered. These axis depend on the forces applied and are difficult to be determined. Because of these difficulties, an assumption has been made that these points are on or near the beam reference line.

In this work, the beam reference axis was maintained fixed, but the wing cross-sections were moved. Doing that, the point of application of aerodynamic loads (quarter chord) and the elastic axis (half chord) were moved in relation to the wing reference axis.

The definition of the local/global flexural axis during maneuvers of very flexible airplanes is difficult. The consideration of one fixed axis, even during maneuvers can contribute to analyze the behavior of flexible airplanes.

The original idea of this work was changing the elastic axis position, related to one fixed point. The NFNS_s formulation allows the changing position of the beam reference line (the beam that describes the wing structural properties). According to the authors understanding, the model and formulation used considers the beam reference line as the line where the representative beam is. This line or this beam transports the wing loads to the fuselage (See Fig. 2). In other words, the beam reference line is coincident with the wing reference axis.

The first idea of this work was to change the relative position between the elastic axis and one fixed point. There are three possible ways of implementing it:

1) Changing the beam reference line and maintaining the wing cross sections fixed. Doing that, the distance from the aerodynamic center to the beam reference line would be changed, and as consequence the pitching moment acting on the aircraft center of gravity could be changed. But, the position of wings center of gravity would also be changed, as the beam representing the wing structure would be moved. And, as consequence, the aircraft center of gravity would be changed also.

2) Maintaining the beam reference line, in order to avoid the changing position of the aircraft center of gravity, and changing position of the wing cross section. Certainly, the aerodynamic center position would change, and also the elastic axis position in reference to one fixed point (the wing beam reference line), but, the distance from the aerodynamic center to the elastic axis would be maintained. According to the wing cross section modeled, it is possible the affirmation that the elastic axis position is located on the center of area of the wing cross section. This does not happen always, but it is true for the beams used here and detailed described by Sousa [12].

3) Changing the beam, with its properties including the structural stiffness and elastic axis position, while maintaining the wing cross sections and beam reference line on the same positions.

In this work, the alternative 2 was used, despite the knowledge that the implementation of this alternative would affect the flight stability also. The alternative 2 was one artificial way of changing the elastic axis position related to fixed points on the beam reference line.

Considering the alternative 2 implemented: maintaining the same beams, the beam reference line and changing position of the wing cross sections, it could be concluded that the aerodynamic center position related to the aircraft center of gravity would be changed, and, as consequence, the moments acting on the center of gravity would be altered also.

Considering the beam reference line fixed to one point on the fuselage while moving the entire wing surface might be considered as moving the beam reference line related to the wing box. This modification on the wing box relative to beam reference line would change the stiffness matrix also. Although the authors understand and accept this concept, in this work, the stiffness matrix was considered constant and diagonal in all simulations. The results obtained were not discrepant from the previous results published in the literature. Some physical explanations related to the results obtained were possible.

This work is organized as follows: Section 1 presented the motivation for the work. Section 2 presents the equations of motion. Section 3 presents the simulated and analyzed aircraft model. Section 4 presents the results and section 5 presents the conclusions.

2. EQUATIONS OF MOTION

The NFNS_s methodology has been continually developed and is described in details in [16,18,5,12,19,20]. A summary of the NFNS_s methodology is described in this part. The equations of motion are obtained with the Principle of Virtual Work [32]. The generalized coordinates consists of the degrees of freedom of the rigid aircraft, the Euler angles, which define the aircraft's orientation relative to earth, aircraft's position also relative to earth, as well as the strains of all elements in the aircraft's structural members. The structural dynamics model uses the strain based formulation [16,22, 4,19,20]. The strain based formulation considers beam's elements with three nodes and 4 local strains: extension ε_x, twist k_x and two bendings k_y, k_z (Fig. 1, Eq.1). These strains are the local degrees of freedom. Fig. 1 illustrates these strains [12].

$$\varepsilon = [\varepsilon_x \quad k_x \quad k_y \quad k_z] \tag{1}$$

The equations of motion of the flexible airplane are obtained with the Hamilton's Principle [16,5,19]. The virtual work of all internal and external forces of all elements are calculated and summed. This total virtual work must be zero. With this consideration, and with the fact that the virtual displacements are arbitrary, the equations of motion are obtained (Eq.2). Equation 3 presents the degrees of freedom of the dynamics modeled.

The virtual work of elastic members is done by the inertial forces, internal structural elastic forces due to the strain and strain rates, external forces and moments.

The complete equations of motion consist of Eq.(2) that contain the dynamics equations together with the rigid body kinematics equations.

where:

- M_{FF} , M_{FB} , M_{BF} , M_{BB} are the components of generalized mass matrix [16,5,19];
- C_{FF} , C_{FB} , C_{BF} , C_{BB} are the components of generalized damping matrix]16,5,19];
- K_{FF} is the stiffness matrix [16,5,19];
- R_F , R_B are the generalized force vectors [16,5,19];
- β =[V, U ,W , q , p , r] is the vector with rigid body degrees of freedom [16,5,19];
- ε is the vector with elastic degrees of freedom [16,5,19];
- ϕ , θ , ψ are the Euler angles [18,12];
- H, p_N , p_E are the components of airplane position in relation to the inertial reference frame [18,12].

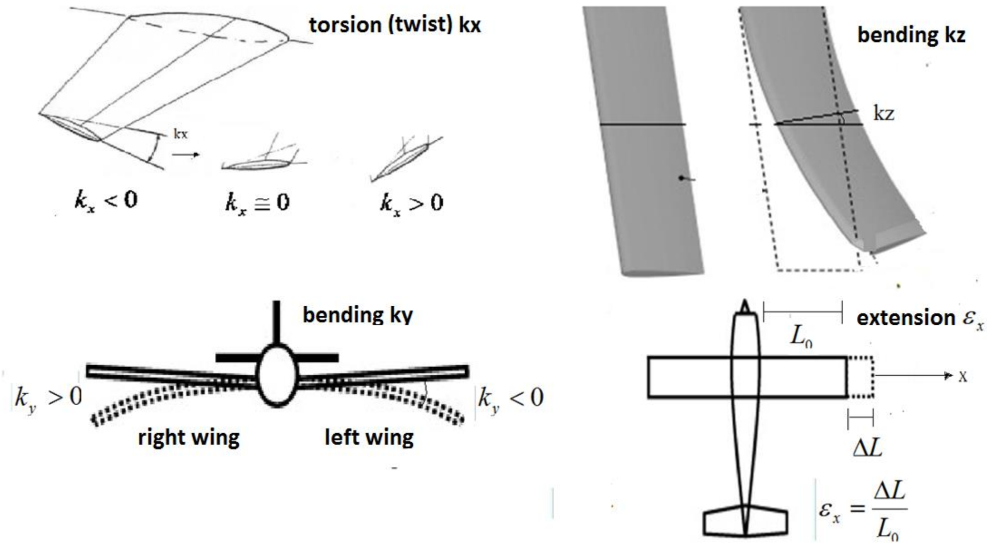

Fig. 1. Strains acting on the structural elements [12],[33], [34]

$$
\begin{aligned}
& M_{FF}\ddot{\varepsilon}+M_{FB}\dot{\beta}+C_{FF}\dot{\varepsilon}+C_{FB}\beta+K_{FF}\varepsilon=R_F \\
& M_{BF}\ddot{\varepsilon}+M_{BB}\dot{\beta}+C_{BF}\dot{\varepsilon}+C_{BB}\beta=R_B \\
& \dot{\phi}=p+\tan(\theta)(q\sin(\phi)-r\cos(\phi)) \\
& \dot{\theta}=q\cos(\phi)+r\sin(\phi) \\
& \dot{\psi}=(q\sin(\phi)-r\cos(\phi))/\cos(\theta) \\
& \dot{H}=U\sin(\theta)-V\cos(\theta)\sin(\phi)+W\cos(\theta)\cos(\phi) \\
& \dot{p}_N=U\cos(\theta)\cos(\psi)+V(-\cos(\phi)\sin(\psi)+\sin(\phi)\sin(\theta)\cos(\psi)-W(\sin(\phi)\sin(\psi)+\cos(\phi)\sin(\theta)\cos(\psi)) \\
& \dot{p}_E=U\cos(\theta)\sin(\psi)+V(\cos(\phi)\cos(\psi)+\sin(\phi)\sin(\theta)\sin(\psi)-W(-\sin(\phi)\cos(\psi)+\cos(\phi)\sin(\theta)\sin(\psi))
\end{aligned}
\tag{2}
$$

$$
q=\begin{bmatrix}\varepsilon\\ b\end{bmatrix}=\begin{bmatrix}\varepsilon\\ p_B\\ \theta_B\end{bmatrix}\quad,\quad \dot{q}=\begin{bmatrix}\dot{\varepsilon}\\ \beta\end{bmatrix}=\begin{bmatrix}\dot{\varepsilon}\\ V_B\\ \omega_B\end{bmatrix}\quad,\quad \ddot{q}=\begin{bmatrix}\ddot{\varepsilon}\\ \dot{\beta}\end{bmatrix}=\begin{bmatrix}\ddot{\varepsilon}\\ \dot{V}_B\\ \dot{\omega}_B\end{bmatrix}
\tag{3}
$$

The NFNS_s methodology considers nonlinear structural dynamics, nonlinear flight dynamics and the inertial couplings. More detailed information about the loads calculated and each term in Eq. (2) can be found [16,18,5,19,20].

3. AIRPLANE MODELED

The modeled vehicle has the properties similar to one medium size jet airplane like Embraer EMB-190/195 and Boeing 737-200/300 [6]. Table 1 presents geometric properties of the airplane. Fig. 2 presents one top view of the airplane. Only the wings and empennages are plotted in this figure. Five structural elements (El.1 to El.5) were considered to each semi-wing, two elements to each half horizontal tail, and one element to the vertical tail. Each element can withstand four deformations like the ones presented in Fig. 1. The fuselage of the airplane analyzed in this paper is considered to be rigid and is modeled as one rigid body annexed to the airplane CG location. The engines are modeled as rigid points appended to one wing node [12]. The aerodynamic, structural and mass distribution data of the airplane simulated in this paper are described in details in Sousa [12]. The mass axis position was considered to be on wing reference axis. According to [27], the coupling between bending and twist modes are decreased when the elastic and mass axis are in the same position. elastic axis positions is located at half wing chord. The wing airfoil is the NACA 2412 (that contains camber), and the total airplane mass is 45000 kg. Wake effects and transonic effects were not considered in this model. Fig. 3 presents the wing reference axis, always fixed in the same position. Fig. 3 presents the lateral view of a wing cross-section. In Fig. 3, the aerodynamic surface is moved, maintaining the beam reference axis fixed. The distribution of mass, inertia and stiffness parameters were maintained constant. The only structural parameter affected by the different position of the wing cross-sections is the elastic axis position in relation to the wing reference axis. Sousa [12] presented the calculus of structural stiffness of the very flexible airplane. The wings and tails were structurally modeled as beams located on the reference axis [31]. The elastic axis position is located on the centroid of the airfoil (wing box). The movement of the wing cross-sections changes the elastic axis position (related to the wing reference axis) and also the point of application of aerodynamic force, in relation also to the wing reference line.

Maintaining the wing reference axis fixed and changing the wing cross-sections (Fig. 3) can alter the flexural axis position, and alter the elastic axis and quarter chord position related to the wing reference axis (beam reference axis). The CG was considered not to change because the wing mass was distributed through the beam reference axis, that is fixed. It should be noted that the distance from the aerodynamic center to the elastic axis are constant, even with the changing position of the wing cross section. The elastic axis of the wing cross sections is located on the center of area of the wing cross sections. The distance altered is the distance from the aerodynamic center to the beam reference line. The beam reference line is supposed to be at or close to the wing local (and/or global) flexural axis. This is one hypothesis assumed by the authors and the results presented in this work, seems to collaborate with the assumption.

The different colors on the legend of Fig. 2 can be seen on simulation results, presented on Figs.09, 11, 13, 17, 19, 21, 26, 27, 28c, 29c. The fuselage was not presented on this figure. Only the wing and horizontal tail.

Fig. 4 presents the airplane frontal view at trimmed condition (V=224.6,m/s, H=10000 m). The dimensions presented on Fig. 4 are in meters. Wing tip deflections close to 1.7 m can be seen. Non-deformed wing and deformed wing are presented.

Table 1. Geometric Properties of modeled airplane

Property	Value
Fuselage Length	33 m
Wing Span	28.4m
Wing Area	95m^2
Wing Sweep (25% mac)	25º
Wing Taper Ratio	0.3
Horizontal Tail Span	11.4m
Horizontal Tail Area	26m^2
Horizontal Tail Sweep	27.5º
Horizontal Tail Taper Ratio	0.45
Vertical Tail Span	5.48m
Vertical Tail Area	20m^2
Vertical Tail Sweep	40º
Vertical Tail Taper Ratio	0.5

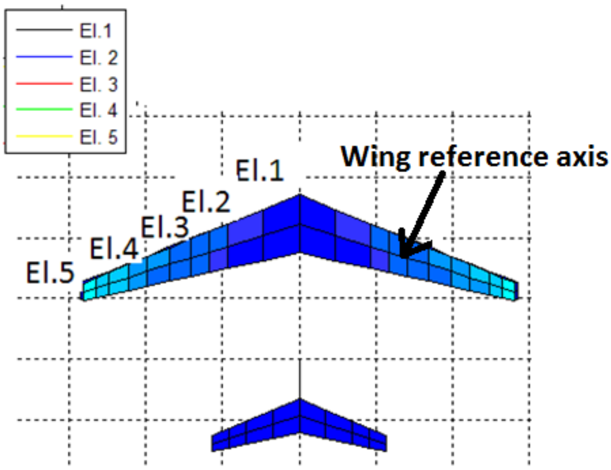

Fig. 2. Structural elements on the wing [12]

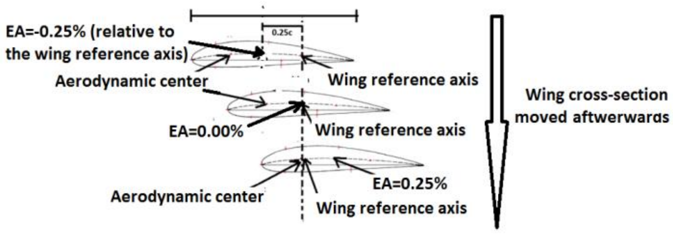

Fig. 3. Airfoil and reference axes

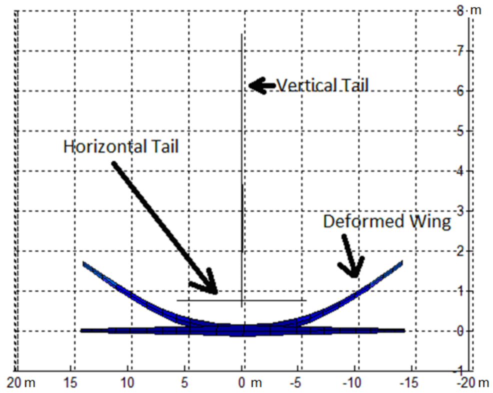

Fig. 4. Frontal view of airplane at trimmed condition

4. SIMULATIONS PERFORMED

The focus of this paper is to evaluate the effects of the elastic axis/ (and flexural axis) position on the flight dynamics and aeroelastic stability on one very flexible transport category airplane. The idea is to make some sensitivity analysis in order to better comprehend the couplings between flight dynamics and aeroelastic stability.

Some simulations with different airspeed values were performed in order to evaluate the effects of airspeed on flight and aeroelastic stability, and to verify the effects of elastic/ flexural axis position on the flight dynamics in different airspeeds.

The simulations presented in this paper are:

1) Calculation of trimmed conditions.

2) Eigenvalues at trimmed conditions.

3) Dynamic simulations.

Table 2 presents the simulated airplane airspeed and structural configurations. All the simulations were performed at initial altitude of 10000 m.:

The cases simulated allowed the verification of effects due to airspeed values and wing elastic axis position in relation to the wing reference axis. The elastic axis is always at half chord of the wing cross-section, but the cross-section can have its position altered in relation to the wing reference axis. The elastic axis position is located at 25% ahead of the wing reference axis (EA=-0.25c), or exactly on the wing reference axis (EA=0.00c) or at 25 % after the wing reference axis (EA=0.25c). The airspeed in all tables and figures in this paper means true airspeed. Although the Mach number for cases 7-9 are 0.657, transonic effects were not considered in the model.

4.1 Trimmed Conditions

Table 3 presents the angle of attack and elevator deflections needed to trim the airplane in cases 1 to 9.

The values of angle of attack are presented also in Table 4. The angle of attack needed to trim the airplane decreases as the wing cross-sections move forward in relation to the wing reference axis. The first explanation thought for this fact is that the forward movement of wing cross sections increases the distance between the aerodynamic center and the beam reference axis position. (See Fig. 22)._As consequence the structural pitch up moment increases, and the twist deformation also. The effective angle of attack is equal to aerodynamic angle of attack minus the angle of attack for zero lift plus the wing incidence. The wing incidence is affected by the twist deformation. Higher twist deformation would cause higher wing incidence and higher effective angle of attack. Then, higher twist would demand less aerodynamic angle of attack (aoa). It could explain the values obtained in Tables 3 and 4. This explanation would be accepted if there was not difference in angle of attack and elevator deflections in case of rigid airplanes. Simulations of rigid airplanes were performed for different values of elastic axis positions (in relation to the wing reference axis), and similar results as that obtained for flexible airplane were seen. Different values for angle of attack and elevator deflections were obtained, despite the fact of almost zero bending and twist deformations. The explanation found is: the values of angle of attack and elevator obtained are function of the moments acting on the airplane center of gravity.

Table 2. Airspeed and wing elastic axis (EA) position

Case	Airspeed	EA pos.
1	124.6 m/s	0.25%c
2	124.6 m/s	0.00 %c
3	124.6 m/s	-0.25%c
4	224.6 m/s	0.25%c
5	224.6 m/s	0.00 %c
6	224.6 m/s	-0.25%c
7	524.6 m/s	0.25%c
8	524.6 m/s	0.00 %c
9	524.6 m/s	0.25%c

Table 3. Trimmed conditions

Case	Angle of attack α (deg)	Elevator δe(deg)
1	15.57	-32.54
2	14.56	-24.20
3	13.62	-16.47
4	2.28	-4.11
5	1.80	-1.31
6	1.35	1.19
7	-2.37	6,00
8	-2.59	6,98
9	-2.82	7.91

Table 4. Values of angle of attack versus airspeed and EA position

	EA=0.25%c	EA=0.00%c	EA=-0.25%c
V(m/s)	aoa (deg)	aoa (deg)	aoa (deg)
124.0	15.57	14.56	13.62
224.0	2.28	1.80	1.35
524.0	-2.37	-2.59	-2.82

In other words, once the distance from the aerodynamic center is altered, the resultant pitching moment acting on the same point is also modified. And this fact justifies the results presented. In summary, here, there is the effect related to the flight stability and not one indirect effect caused only by aeroelastic stability.

The afterward displacement of the wing cross-section decreases the control authority, and demands more elevator to trim the airplane. And the opposite is true: the forward displacement of wing cross-section increases the control authority. Note that less elevator is needed to trim the airplane or to command nose up when the wing reference axis is closer to the trailing edge and one little more elevator is needed to command nose down. But the difference is higher when it is considered nose up maneuvers.

This happens due to the fact that the pitching moment used in equations of motion act on the wing reference axis position. It means that for higher the value of wing reference axis position in relation to the wing trailing edge, higher will be the nose up wing pitching moment due to distance between the aerodynamic center and the wing reference axis (See Fig. 22). So lower will be the negative (or higher will be the positive) wing pitching moment. As consequence, less Nose Up (or higher Nose Down) elevator deflection will be needed to balance the wing pitching moment. The results presented in Table 4 and in Fig. 4 present the same tendency as the ones verified in [26]. In that reference, the methodology of Tuzcu, Meirovitch [13,14] was used to implement the mathematical model. The fact of two different methodologies present similar results seems to be one validation of the results obtained here.

4.2 Stability Analysis

The eigenvalues related to aeroelastic and rigid body dynamics were calculated for the trimmed conditions of cases 1 to 9 of Table 2.

Table 5. Eigenvalues calculated at trimmed condition

	V=124.6m/s	V=224.6 m/s	V=524.6m/s
Eigenvalues – Aeroelastic dynamics, EA = 0.25c	-8.5410 +26.4505i	-9.9057 +26.5427i	-9.0945 +33.0075i
	-8.5410 -26.4505i	-9.9057 -26.5427i	-9.0945 -33.0075i
	-8.4009 +26.1600i	-9.8625 +26.5481i	-6.3058 +35.0825i
	-8.4009 -26.1600i	-9.8625 -26.5481i	-6.3058 -35.0825i
	-3.8676 +18.0366i	-5.0977 +20.5785i	-4.7967 +34.8901i
	-3.8676 -18.0366i	-5.0977 -20.5785i	-4.7967 -34.8901i
	-3.7003 +17.7258i	-4.8852 +20.0799i	-1.9205 +11.4381i
	-3.7003 -17.7258i	-4.8852 -20.0799i	-1.9205 -11.4381i
	-1.5725 + 9.0068i	-2.0841 + 9.9730i	-1.9071 +11.3670i
	-1.5725 - 9.0068i	-2.0841 - 9.9730i	-1.9071 -11.3670i
	-1.6037 + 9.0871i	-2.1261 +10.0743i	
	-1.6037 - 9.0871i	-2.1261 -10.0743i	
Eigenvalues – Rigid Body dynamics, EA = 0.25c	-0.2329 + 1.2015i	-2.1488	-1.1425 + 5.1878i
	-0.2329 - 1.2015i	-0.4814 + 2.2125i	-1.1425 - 5.1878i
	-0.1515 + 1.2891i	-0.4814 - 2.2125i	-5.2360
	-0.1515 - 1.2891i	-0.0965 + 1.5483i	-0.2004 + 3.4756i
	-0.7776	-0.0965 - 1.5483i	-0.2004 - 3.4756i
	-0.0001 + 0.1150i	-0.0020 + 0.0696i	-0.0032 + 0.0425i
	-0.0001 - 0.1150i	-0.0020 - 0.0696i	-0.0032 - 0.0425i
	-0.0002	-0.0053	-0.0065
	0.0025	-0.0010	0.0005
Eigenvalues – Aeroelastic dynamics, EA = 0.00c	-8.5711 +26.4502i	-4.8597 +20.4723i	**0.6347 +36.2712i**
	-8.5711 -26.4502i	-4.8597 -20.4723i	**0.6347 -36.2712i**
	-8.4052 +26.1150i	-4.6571 +19.8904i	-9.1252 +31.0465i
	-8.4052 -26.1150i	-4.6571 -19.8904i	-9.1252 -31.0465i
	-3.7876 +17.9723i	-2.2022 +10.1464i	**0.9971 +36.0695i**
	-3.7876 -17.9723i	-2.2022 -10.1464i	**0.9971 -36.0695i**
	-3.6201 +17.6594i	-2.2484 +10.2569i	-9.8417 +31.9578i
	-3.6201 -17.6594i	-2.2484 -10.2569i	-9.8417 -31.9578i
	-1.6150 + 9.0311i		-1.9883 +11.8634i
	-1.6150 - 9.0311i		-1.9883 -11.8634i
	-1.6453 + 9.1068i		-1.9757 +11.7760i
	-1.6453 - 9.1068i		-1.9757 -11.7760i
Eigenvalues – Rigid Body dynamics, EA = 0.00c	-0.2307 + 1.1051i	-2.2467	-5.4080
	-0.2307 - 1.1051i	-0.4745 + 2.0134i	-1.1262 + 4.7102i
	-0.1466 + 1.2715i	-0.4745 - 2.0134i	-1.1262 - 4.7102i
	-0.1466 - 1.2715i	-0.0793 + 1.5404i	-0.1937 + 3.4725i
	-0.8276	-0.0793 - 1.5404i	-0.1937 - 3.4725i
	0.0001 + 0.1146i	-0.0019 + 0.0693i	-0.0032 + 0.0423i
	0.0001 - 0.1146i	-0.0019 - 0.0693i	-0.0032 - 0.0423i
	-0.0002	-0.0010	-0.0065
	0.0021	-0.0057	0.0005
Eigenvalues – Aeroelastic dynamics, EA = -0.25c	-8.6125 +26.4413i	-4.5746 +20.3088i	**5.9859 +34.3594i**
	-8.6125 -26.4413i	-4.5746 -20.3088i	**5.9859 -34.3594i**
	-8.4199 +26.0660i	-4.4006 +19.6346i	**6.1903 +34.2713i**
	-8.4199 -26.0660i	-4.4006 -19.6346i	**6.1903 -34.2713i**
	-3.7150 +17.8953i	-2.3352 +10.3599i	-8.9065 +30.2687i
	-3.7150 -17.8953i	-2.3352 -10.3599i	-8.9065 -30.2687i
	-3.5480 +17.5792i	-2.3872 +10.4859i	-9.3506 +30.9514i
	-3.5480 -17.5792i	-2.3872 -10.4859i	-9.3506 -30.9514i
	-1.6587 + 9.0570i		-2.0681 +12.3023i
	-1.6587 - 9.0570i		-2.0681 -12.3023i
	-1.6880 + 9.1287i		-2.0569 +12.2036i
	-1.6880 - 9.1287i		-2.0569 -12.2036i

	V=124.6m/s	V=224.6 m/s	V=524.6m/s
Eigen Values – Rigid Body dynamics, EA = -0.25c	-0.2295 + 0.9985i	-2.3474	-5.5899
	-0.2295 - 0.9985i	-0.4693 + 1.7920i	-1.1139 + 4.1770i
	-0.1407 + 1.2540i	-0.4693 - 1.7920i	-1.1139 - 4.1770i
	-0.1407 - 1.2540i	-0.0616 + 1.5331i	-0.1853 + 3.4678i
	-0.8803	-0.0616 - 1.5331i	-0.1853 - 3.4678i
	0.0003 + 0.1140i	-0.0019 + 0.0689i	-0.0032 + 0.0419i
	0.0003 - 0.1140i	-0.0019 - 0.0689i	-0.0032 - 0.0419i
	-0.0002	-0.0010	-0.0065
	0.0016	-0.0062	0.0003

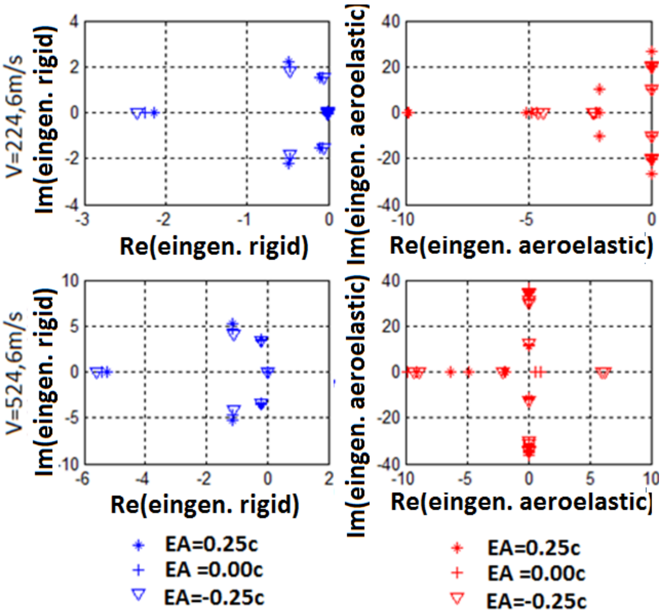

Fig. 5. Eigenvalues calculated for cases 1 to 6

The results obtained showed that flutter occurs in cases 4 and 6. Airspeed = 524.6 m/s and EA = 0.00c and -0.25c, respectively. More aft the flexural axis position (in relation to the aerodynamic center), lower values of damping are found and more severe is the flutter. It is equivalent to say that the more aft the EA position, lower will be the flutter speed. Remark: EA=-0,25% means all the points of wing section were moved forward in relation to the beam reference line/ flexural axis. It means the distance between the aerodynamic center and the flexural axis is higher (See Figs. 2-3). From the point of view of a fixed reference point on the wing section, the flexural axis would have moved backwards.

The values obtained in Table 5 were used to plot the eigenvalues related to "rigid" body dynamics and aeroelastic dynamics on Fig. (5). Four graphics were plotted. The plots contain the eigenvalues related to rigid body dynamics (blues plots, first column) and aeroelastic dynamics (red plots, second column). The first line contains the eigenvalues obtained for the airspeed of 224.6m/s and the second line shows the eigenvalues obtained for the airspeed of 524.6m/s. In each plot, the eigenvalues obtained for the elastic axis positions (EA) = 0.25c, 0.00c, and -0.25c are presented. Table 5 presents the unstable aeroelastic eigenvalues on third and fifth line, fourth column (underlined and bold). The coalescence of two modes can be seen at V=524.6m/s, EA = 0.00c, and -0.25c. This coalescence seems to increase as the wing cross sections is moved forwards in relation to the wing reference axis. Remark: The coalescence is noted due to the fact the two pairs of eigenvalues are quasi coincident.

Using the eigenvalues obtained (presented on Table 5, the values of damping ratio and undamped natural frequency of short period, dutch roll and phugoid modes were calculated. These values are presented in Tables (6) and (7). These tables contain the damping and frequency obtained for the airspeeds 224.6m/s and 524.6m/s, respectively. It should be noted in Fig. 5 that some elastic eigenvalues appear to have a null value, but looking at eigenvalues obtained and presented on Table 5, it can be said that this is not the case. Some points with positive eigenvalues were noticed, but with small amplitudes. And points in conditions where no flutter was found (points underlined in black in Table 5). This may indicate fine adjustments needed in the calculation of eigenvalues. Nevertheless, the points underlined and highlighted in red correspond to situations in which flutter occurred. This was seen in the dynamic simulations.

The values presented in Tables 5-7 show that:

a) The damping of short period increases a little with airspeed and increases with the displacement of wing reference axis towards the trailing edge, or, more precisely, with the forward displacement of the wing cross-section;

b) The frequency of short period mode increases too much with the airspeed and decreases with the forward displacement of cross-sections;

c) The damping of dutch roll decreases with airspeed and decreases with the forward displacement of wing cross-sections;

d) The frequency of dutch roll mode increases too much with the airspeed and does not suffer any significant change as position of the wing cross-section is altered;

e) The damping of phugoid increases too much with airspeed and decreases a little with the displacement of wing cross-section;

f) The frequency of phugoid mode decreases with the airspeed and decreases a little with the forward displacement of the wing cross-section;

g) The aeroelastic stability decreases with the forward displacement of wing cross-section. The positive real values of aeroelastic eigenvalues increases. See fourth graphic on Fig. (6).

4.3 Dynamic Simulations

Figs. (6) to (21) present the airplane response to one doublet of elevator. The figures contain the plots of elevator deflection δp (deg), pitch rate q(deg/s), airspeed V (m/s), altitude H(m), bending strain ky (rad) and twist strain kx (rad) in function of time t(s). The plots of deformations contain the values of strains on five elements on left and right semi-wings. The black, blue, red, green and yellow plots (in Figs. 9, 11, 13, 17, 19, 21) present the values calculated for the elements 1 to 5, respectively. Structural element 1 is on the wing root, and element five is on the wing tip. The other elements are intermediary (See Fig. (2)). The plots of deformed airplane at trimmed condition are also presented in Figs. 6-7, 14-15. In these figures, perspective and frontal views of the trimmed airplane are presented.

Fig. 6 presents one perspective view of the airplane trimmed at 224.6m/s, 10000 m and EA=0.00c. Fig. 7 presents the frontal view. High value of UP wing bending ky can be seen. The units in all axes are meters.

Table 6. Values of damping factor and natural frequency, true Airspeed=224,6m/s, EA=25%c, 0.00%c, -25%c

	Short Period		Dutch Roll		Fugoid	
	ζ	**wn**	**ζ**	**wn**	**ζ**	**wn**
EA= 0.25c	0.213	2.26	0.0622	1.55	0.0287	0.0696
EA = 0.00c	0.229	2.07	0.0514	1.54	0.0274	0.0693
EA = --0.25c	0.253	1.85	0.0401	1.53	0.0276	0.0689

Table 7. Values of damping factor and natural frequency, true airspeed = 524,6m/s, EA=25%c, 50%c, 75%c

	Short Period		Dutch Roll		Fugoid	
	ζ	**wn**	**ζ**	**wn**	**ζ**	**wn**
EA= 0.25c	0.215	5.31	0.0576	3.48	0.0751	0.0426
EA = 0.00c	0.232	4.84	0.0577	3.48	0.0754	0.0424
EA = --0.25c	0.258	4.32	0.0534	3.47	0.0762	0.0420

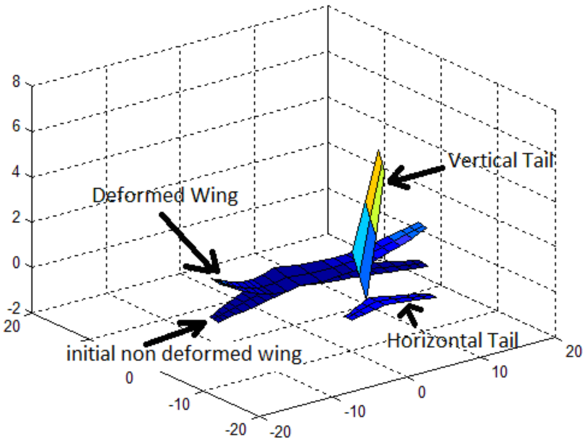

Fig. 6. Airplane at trimmed condition – 224.6m/s, 10000 m, EA=0.00 c. Perspective

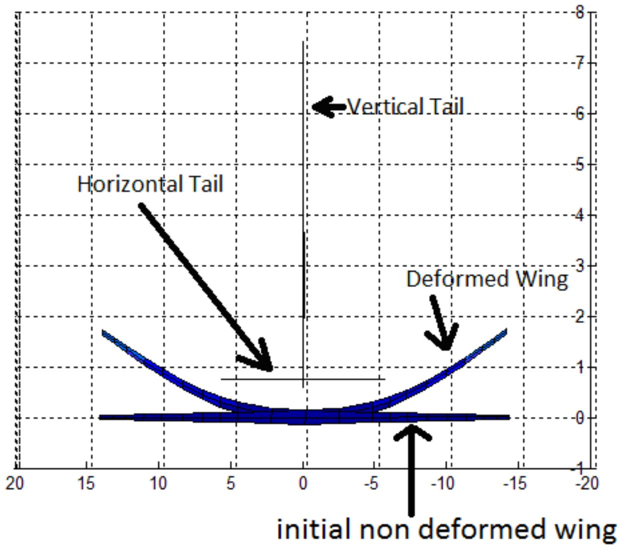

Fig. 7-Airplane at trimmed condition – 224.6m/s, 10000 m, EA=0.00 c., frontal view

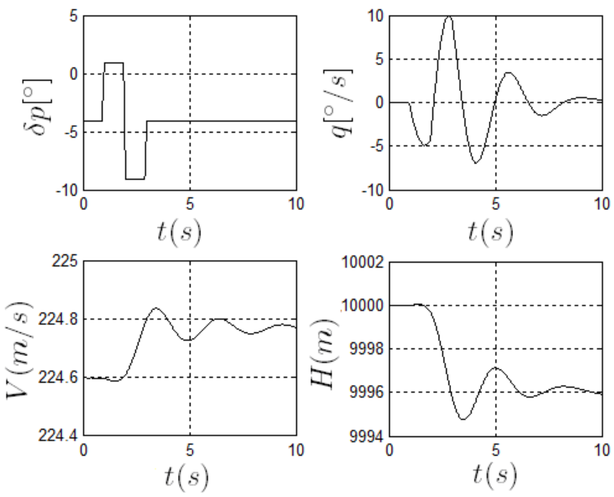

Fig. 8. Airplane Response to one doublet of elevator, V=224.6m/s, EA=0.25 c

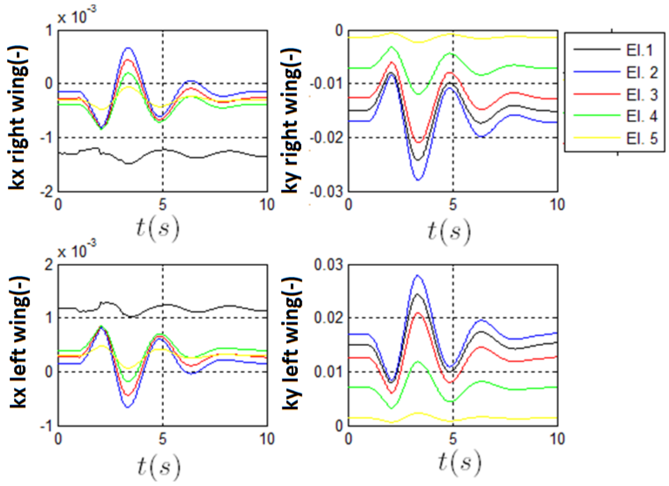

Fig. 9. Bending and Twist Wing response to one doublet of elevator, V=224.6m/s, EA=0.25 %c

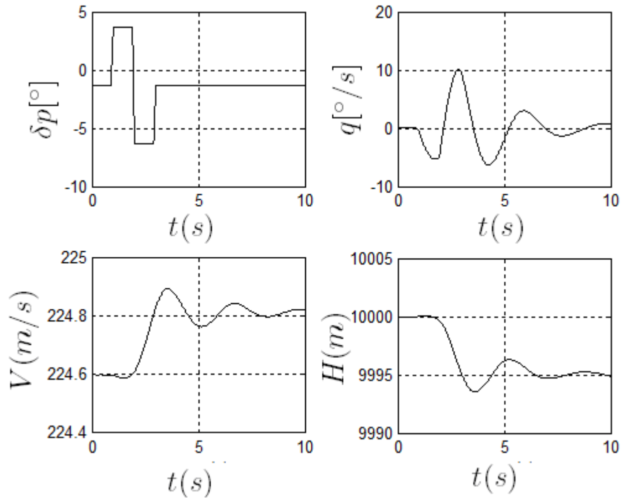

Fig. 10. Airplane Response to one doublet of elevator, V=224.6m/s, EA= 0.00c

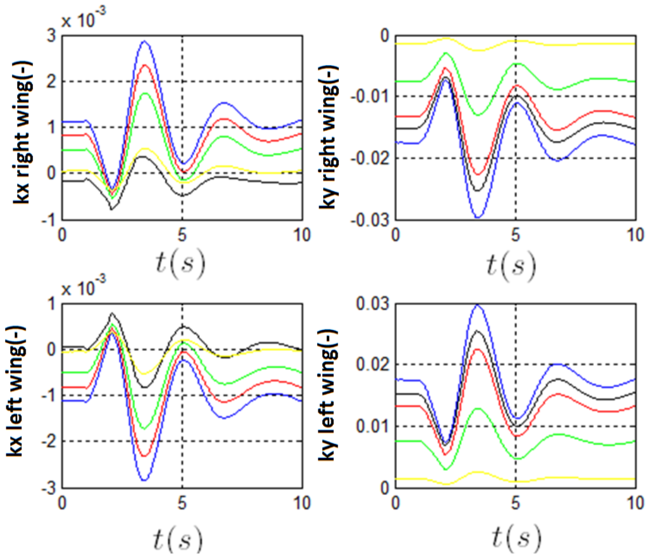

Fig. 11. Bending and Twist Wing response to one doublet of elevator, V=224.6m/s, EA= 0.0 c

Figs. 8 and 9 contain the airplane response to the elevator deflection commanded. The trimmed airspeed is V=224.6m/s. The elastic axis position is located at 25 %c afterwards of the wing reference axis (EA=0.25c). (See Fig. 3). The wing reference axis (flexural axis) are closer to the aerodynamic center.

Figs. 10 and 11 contain the airplane response to the elevator deflection commanded. The trimmed airspeed is V=224.6m/s. The elastic axis position is located at the same position of the wing reference axis (EA=0.00c).

Figs. 12 and 13 contain the airplane response to the elevator deflection commanded. The trimmed airspeed is V=224.6m/s. The elastic axis position is located at 25 %c forwards of the wing reference axis (EA=-0.25c). The wing reference axis (flexural axis) is more AFT in relation to the aerodynamic center. (See Fig. 3).

Remark: The wing reference axis was maintained constant in relation to the airplane center of gravity, and the wing surface was moved in relation to the wing reference axis (beam reference line) as presented in Fig. 3. Despite that, only the relative movement of the wing reference axis to the wing aerodynamic center was considered in the following analyses.

The comparisons of Figs. 8,10,12 and 9,11,13 shows that:

a) The initial bending deformations are not changed significantly at trimmed condition, i.e, the position of wing reference axis (related to the point of application of aerodynamic loads) did not bring any significant difference to ky at trimmed condition;

b) The initial twist deformations were significantly altered with the modification of wing reference axis. More aft this axis (in relation to the aerodynamic center), higher initial twist strain (kx).

c) The amplitudes of bending deformations during the transient response were a little modified by the changing of wing reference axis. More aft the axis (in relation to the aerodynamic center), a little higher the amplitude of bending ky.

d) The amplitudes of twist deformations during the transient response were modified with the changing of wing reference axis. More aft the axis, higher the amplitude of twist kx.

e) The pitch rate response to the elevator command was not modified. In other words, it seems that the elevator efficiency was not modified with the modification of wing reference axis position;

f) The pitch rate damping was a little increased as the wing reference axis is moved to aft position.

g) The twist and bending deformations are in phase.

h) In all these simulations, the airplane presents aeroelastic dynamic stability. There is no flutter.

Considering the wing reference axis at or close to the flexural axis, the relative distance between the point of application of aerodynamic loads (quarter chord) to the wing flexural axis could justify the behavior observed.

Fig. 14 presents one perspective view of the airplane trimmed at 524.6m/s, 10000 m and EA=0.00c. Fig. 15 presents the frontal view. The DOWN wing bending ky can be seen. DOWN wing twist also was obtained.

Figs. 16 and 17 contain the airplane response to the elevator deflection at trimmed condition, (V=524.6m/s). The elastic axis position is located at 25 % of the mean aerodynamic chord (EA=0.25c).

Figs. 18 and 19 contain the airplane response to the elevator deflection at trimmed condition, (V=524,6m/s). The wing reference axis is located at 50 % of the mean aerodynamic chord (EA=0.00c). The occurrence of flutter can be seen on Figs. 18 and 19.

Figs. 20 and 21 contain the airplane response to the elevator deflection at trimmed condition, (V=524.6m/s). The wing reference axis is located at 75 % of the mean aerodynamic chord (EA=-0.25c). The occurrence of flutter can also be seen.

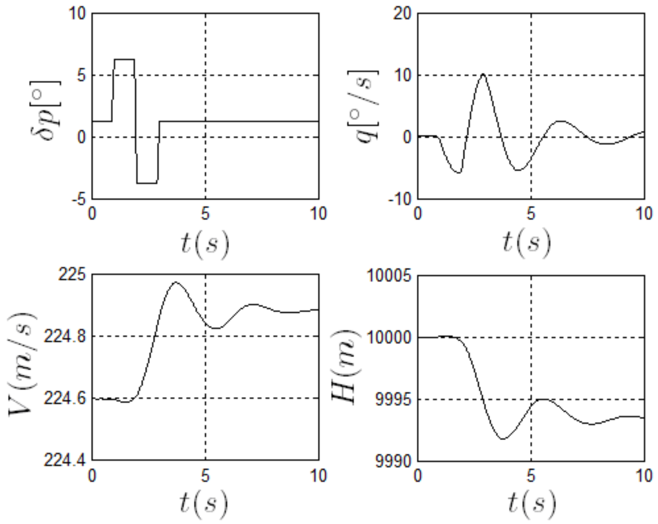

Fig. 12. Airplane Response to one doublet of elevator, V=224.6m/s, EA= -0.25c

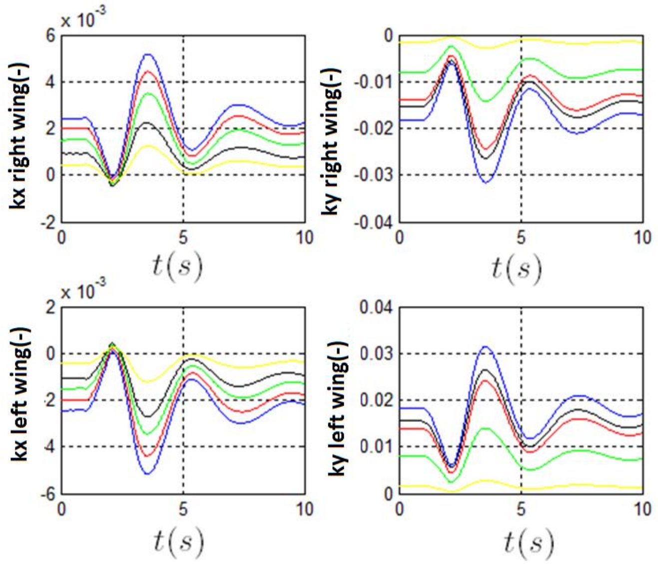

Fig. 13. Bending and Twist Wing response to one doublet of elevator, V=224.6m/s, EA=-0.25c

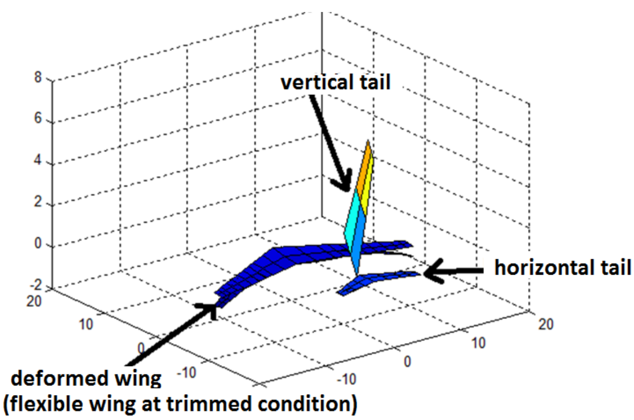

Fig. 14. Airplane at trimmed condition – 524.6m/s, 10000 m, EA= 0.00 %c., perspective

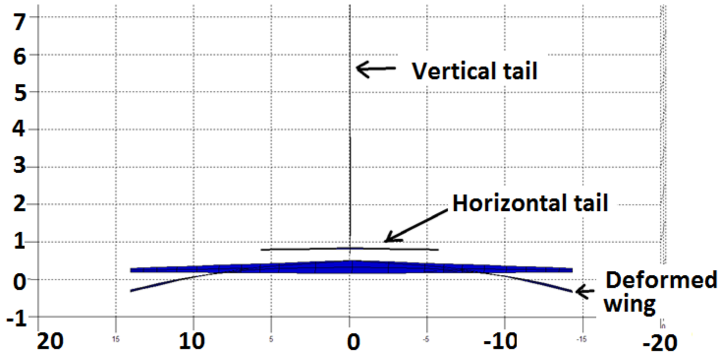

Fig. 15. Airplane at trimmed condition – 524.6m/s, 10000 m, EA=0.00 c., frontal View

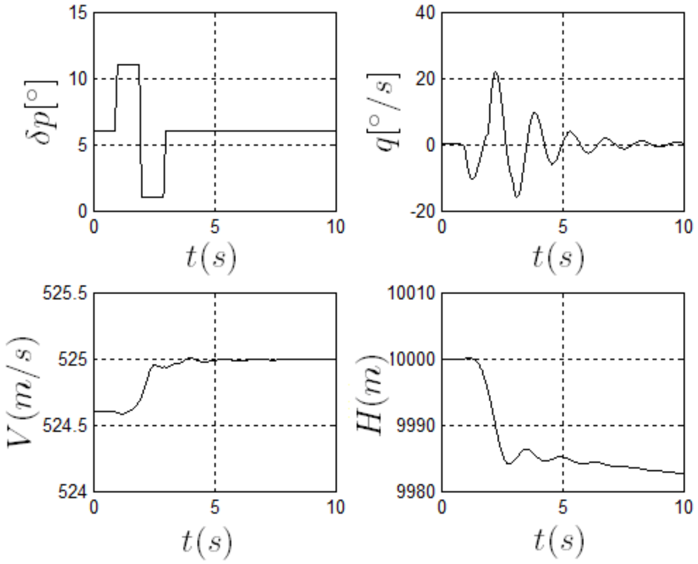

Fig. 16. Airplane Response to one doublet of elevator, V=524.6m/s, EA=0.25 c

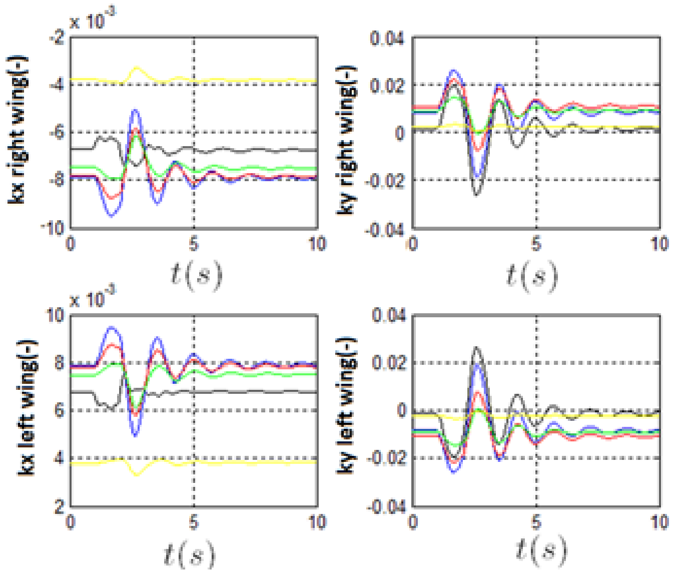

Fig. 17. Bending and twist wing response to one doublet of elevator, V=524.6m/s, EA= 0.25 c

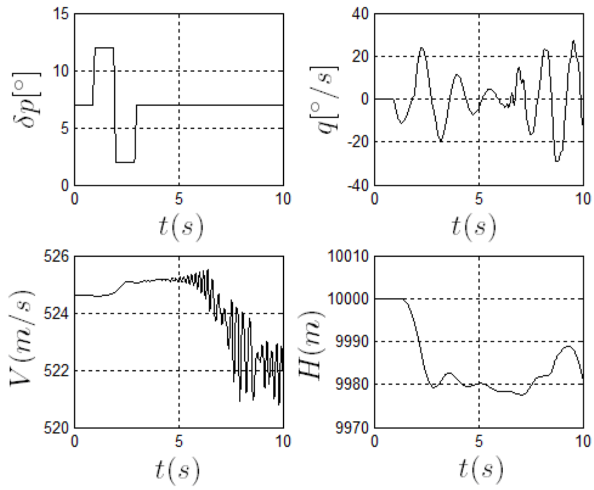

Fig. 18. Airplane response to one doublet of elevator, V=524.6m/s, EA= 0.00 c

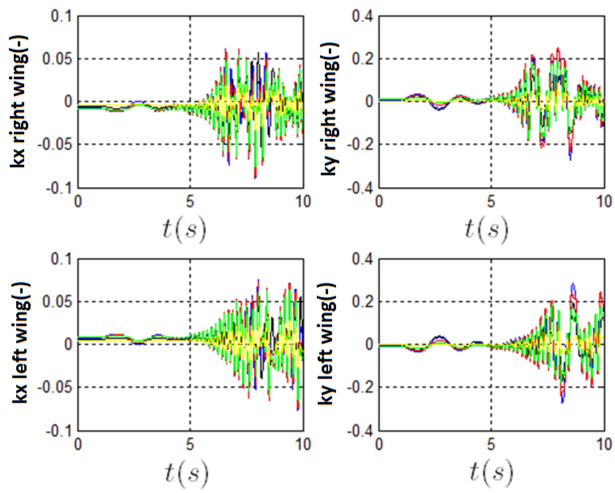

Fig. 19. Bending and Twist Wing response to one doublet of elevator, V=524.6m/s, EA= 0.00 c

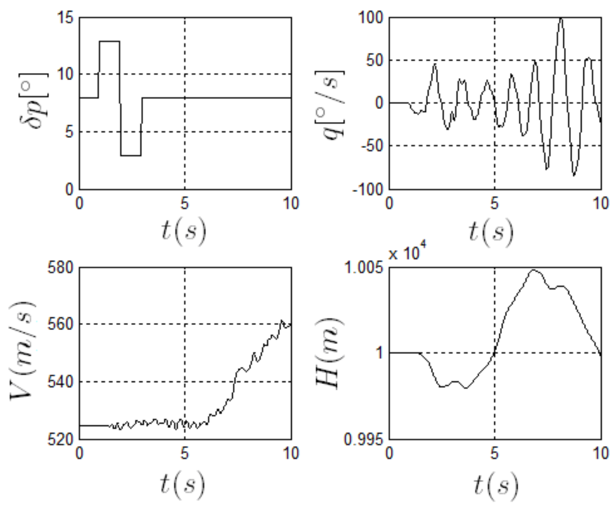

Fig. 20. Airplane Response to one doublet of elevator, V=524.6m/s, EA= -0.25c

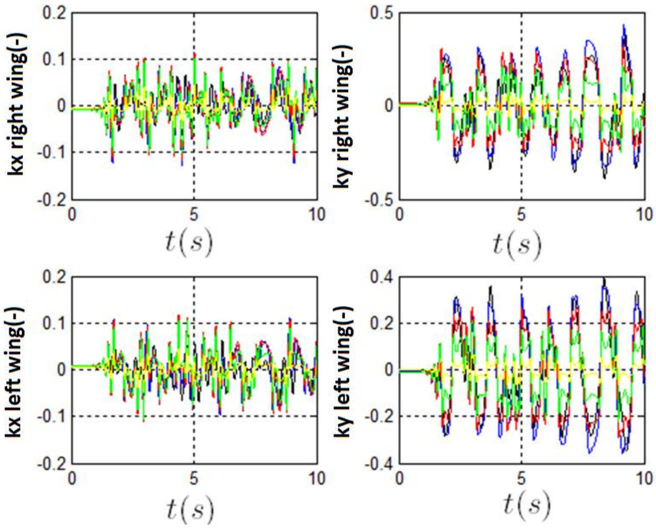

Fig. 21. Bending and Twist Wing response to one doublet of elevator, V=524.6m/s, EA= -0.25 c

The comparisons of Figs. 16, 18, 20 and 17, 19, 21, shows that:

a) The relative displacement of the wing reference axis towards the trailing edge decreases the aeroelastic stability.

b) The flutter can be seen in Figs. 19 and 21. More aft the wing reference axis, more severe is the flutter.

c) The wing bending strain is much higher than the twist strain when there is no flutter (Fig. 16). The ratio bending ky/twist kx is of the order of 10.

d) The wing bending strain amplitude is only three to four times of wing twist strain when there is flutter (Figs. 19 and 21).

e) The twist and bending deformations are in phase when there is no flutter (Fig. 17), but presents phase difference when there is flutter (Figs. 19 and 21).

f) Phase difference can be seen in Figs. 19 and 21. In Fig. 21, the difference of phase is higher.

g) Higher the phase difference, more severe is the flutter.

h) When there is flutter, violent oscillations in pitch rate can be seen.

Considering the wing reference axis at or close to the flexural axis, the results could be expected, once the distance between the aerodynamic quarter chord to the flexural axis can be used to describe the results observed.

5. ANALYSIS OF RESULTS

In the last item, it could be seen that the bending and twist deformations were in phase when there was no flutter. The explanation for this is that the aerodynamic was considered to be quasi-steady. Wake effects were not considered. So, the effects of strains on aerodynamic loads would be instantaneous, without time delay.

The analysis presented in the next items will consider the hypothesis that the wing reference axis are at or close to the flexural axis.

The effect of position of flexural axis was clearly seen. Basically, when the flexural axis is located close to the leading edge (more forward), the airplane is more stable. In other words, the flutter speed will be higher. And, when more aft the flexural axis is located, lower will be the flutter speed.

Fig. 22 shows a two dimensional airfoil. The pitch moment M act on the flexural axis (axis of rotation), and will increase if the flexural axis position moves towards the trailing edge. So, the nose up twist deformation will be higher.

In this case, if only the twist deformation is considered, it can be seen that this situation could be considered “aerodynamically unstable”. The positive pitching moment causes one positive twist, that increases the lift force and the pitching moment, and for this time this increases more the twist. What limits the twist deformation is the wing torsion (twist) stiffness. The idea here is that if the wing suffers one external perturbation, whose effect is the increasing in lift force, the twist deformation seems to amplify this effect. And this amplification will be higher, as the flexural axis is moved towards the trailing edge.

On the other hand, if the Figs. 23 and 24 are seen, it can be thought that the bending deformations ky can act to damp the effects of external perturbations.

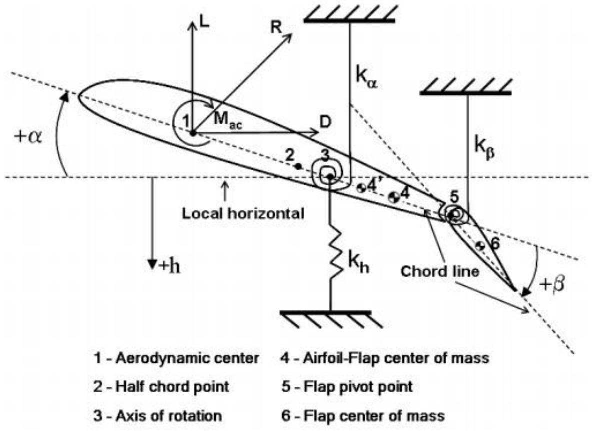

Fig. 22. Two dimensional airfoil [35]

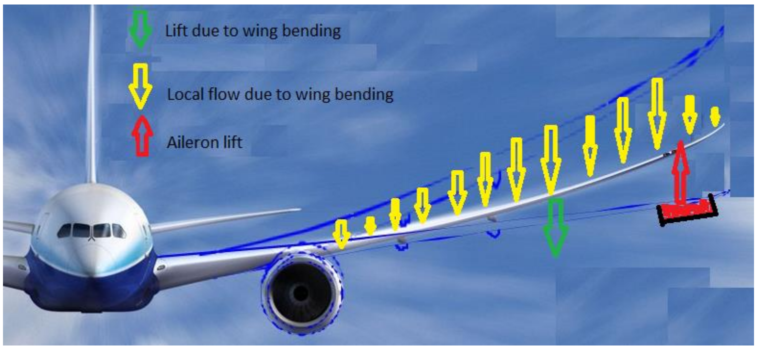

Fig. 23. Damping in external perturbations due to bending deformations [12, Adapted from 36]

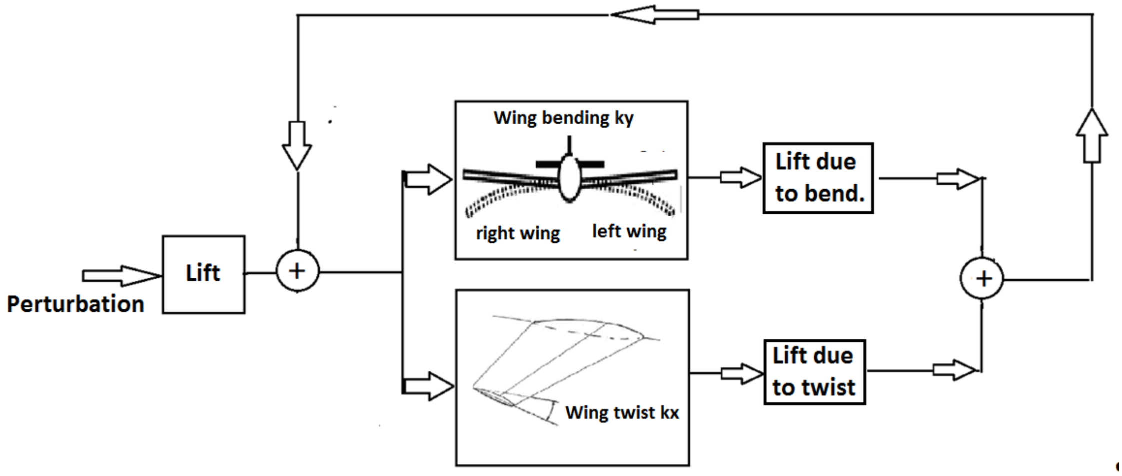

Fig. 24. Mechanism for amplification or damping of structural deformations

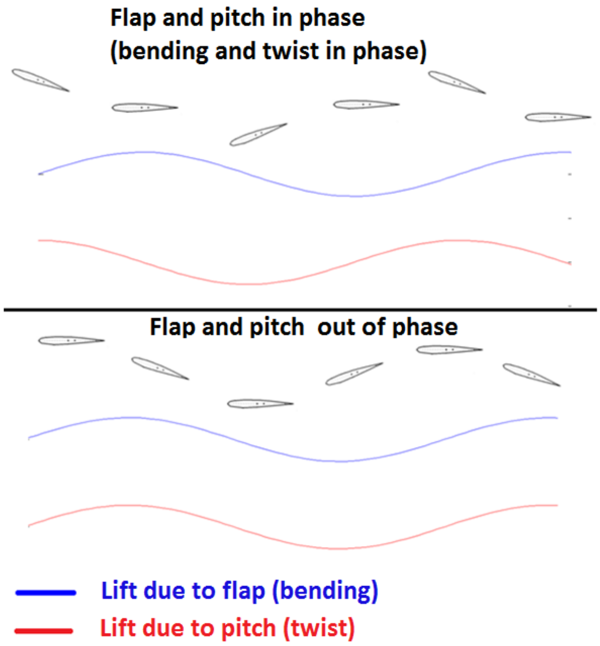

Fig. 25. Example of phase difference between the pitch and flap movements

.

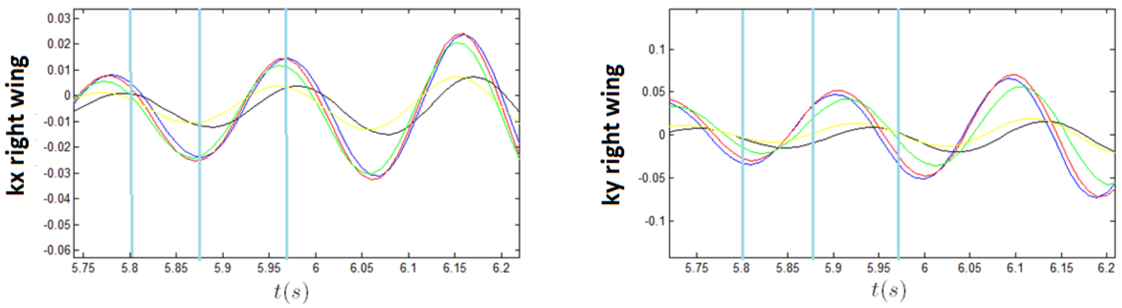

Fig. 26. Phase difference between bending and twist deformations – Close view – Fig. 19

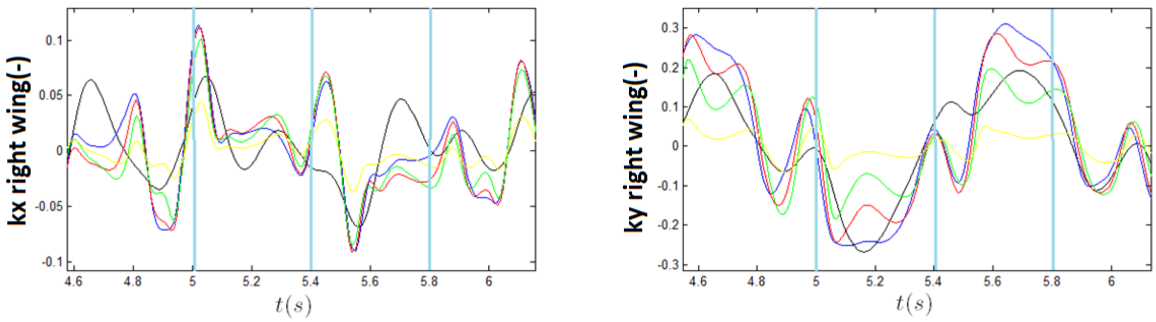

Fig. 27. Phase difference between bending and twist deformations – Close view – Fig. 21

Consider the situation in which the aileron was deflected downwards and this deflection increased the lift force on left wing (red arrow in Fig. 23). If the airplane is very flexible, the left wing will moves up (here only the bending is being considered). As a result, there will be one local flow related to this bending (yellow arrow on Fig. 23). It will cause one lift force with opposite direction of what was commanded (see green arrow). This figure can be used to conclude that external perturbations could be damped by the bending deformations, if wake effects were not considered.

These comments indicate that the twist and bending deformations seen to act in opposite directions. The twist seems to amplify the external deformations and the bending try to damp. Obviously, the structural stiffness limits these deformations.

When the bending and twist deformations are in phase, one increase in lift force will increase both deformations. But the lift due to positive twist will be positive and the lift due to bending will be negative. It could be thought that the modification in lift force due to the twist and due to bending deformations would cancel each other.

Fig. 24 shows what happens in flexible airplanes (only the first pure bending and pure torsion modes are being considered). When the airplane suffers one perturbation (control surfaces deflections, gusts, turbulence), there are changes in lift force. In case of flexible airplanes, there will be bending and twist deformations, and as consequence, variations on lift force due to bending and due to twist. These variations in lift force act on the airplane. If the twist and bending deformations are in phase, the variation on lift force due to the deformation can be much lower than the initial lift force. If the twist and bending contains difference of phase, the variation on lift force can amplify the wing deformations, and, as consequence the lift force can be increased more. And this increased force, for this time, increases the deformations. In other words, there would be aeroelastic instability.

Fig. 25, shows the idea of phase difference.

In first situation, the flap (bending) deformation is maximum at the same time that the pitch (twist) deformations maximum. As consequence, in this instant of time, the lift due to flap will be negative, and lift due to pitch will be positive. These two forces will help to cancel each other, or, at least, to decrease the delta (variation on) lift force shown on Fig. 24. In this case, the airplane would not present flutter. Note that it is exactly this situation that was verified on simulations presented on Figs. 09, 11, 13 and 17.

Here, it must be remembered that right wing bending UP, correspond to negative values, and right wing twist UP correspond to positive values. It occurs due to the axis system used. More details, see [12]. This fact explains why the twist and bending deformations present opposite signals.

The second situation on Fig. 25 show one situation in which the flap (bending) and pitch (twist) deformations contains one difference of phase of 90 deg. The pitch (twist) is zero when the flap (bending) is maximum or minimum. And the pitch (twist) is maximum or minimum when there is no bending. In this situation, the delta lift force (variation on lift force) due to bending will not cancel or decrease the delta lift force due to twist. The delta lift forces will be added, and this will increase the initial lift force. In consequence, the bending and twist will increase. There would be aeroelastic instability.

The main idea is that phase difference contributes significantly to the occurrence of flutter.

Figs. 26 and 27 presents one close view of right wing bending and twist deformations, presented before on Figs. 19 and 21, respectively. The first plot present the twist deformations kx on the five structural elements of right semi-wing, and the second plot presents the right semi-wing bending deformations ky. If the values presented on Fig. 26, at instants of time t=5.8s, t=5.87s, and t=5.97 s are observed, the difference of phase can be noted. At t=5.8 s, the blue and red plots present very small twist and minimum bending (high amplitude and negative signal). At instant of time t=5.87s, one difference of phase of the order of 135 deg can be seen. The twist observed on blue, green and red plots are in maximum negative value, and the bending observed are in one intermediary value between the null bending and maximum bending. And at t=5.97s, one difference of phase of 135 deg is seen again. This situation corresponds to the second situation presented on Fig. 26. And the airplane presented flutter on the case simulated, as was presented on Fig. 19.

Fig. 27 presents one close view of results contained in Fig. 21. The flutter presented on Fig. 21 were much more severe than the flutter on Fig. 19. In Fig. 27, differences of phase can be observed, but the “behavior” of the oscillations seems to be much more irregular than the behavior presented on Fig. 25. If the bending and twist amplitudes are analyzed on time instant t=5,0 s, it seems the bending and twist have one different of phase lower than 40 deg. At time t=5,4s; it seems that the oscillations have one difference of phase of 90 deg. The twist kx is close to the zero amplitude and the bending ky is on the maximum value. At t=5.8s, it seems the twist and bending seems to present difference of phase higher than 180 deg. The twist seems to be on the more negative value and preparing to increase its value, while the bending passed the maximum amplitude value and is decreasing its value.

Other fact to be noted is that it seems there are oscillations with different and higher (multiple) frequencies added to the dynamics. This can be expected, once there are different natural modes with different frequencies.

The observations made in the Figs. 06 to 21 and the comments presented show that the flutter is related to phase difference and to couplings of different natural modes. Other fact noted is that the twist and bending deformations change too much its oscillations when there is flutter. The ratio of twist/bending amplitudes increase significantly when there is flutter. The phase difference also increases.

The effects can be justified by the distance between the point of application of aerodynamic loads to the flexural axis. This fact allows the proposition that the wing reference axis is at or close to the wing flexural axis.

The effects of flexural axis position on flutter speed presents the same tendency as the one presented on Wright and Cooper [27].

Once verified these effects, it can be concluded that elastic axis and flexural axis positions are important parameters to be analyzed during the project and development of flexible airplanes.

Considering the wing reference axis as the local flexural axis, or close to, all results obtained could be attributed to the local flexural axis position.

Despite the analysis presented, the airplane modeled has wing sweep, and, for this reason, it could thought the sweep is responsible by some of the effects observed. In order to verify it, similar simulations were performed with the same airplane, but with zero wing sweep (See Figs. 28 and 29). The results obtained and presented in the following pages demonstrated that the (down) twist of the wing cross-sections has lower amplitude than that obtained with wing sweep. It could mean that the mechanism used for damp the wing aeroelastic oscillations would be weaker. As consequence, the flutter speed would be lower. This was verified in the simulations performed, and according to Bisplinhoff and Ashley [37], these results are expected in theory. The simulations with the airplane without wing sweep are presented in Figs. 28-29.

In Fig. 28c, it can be noted that the initial twist amplitude (kx) of elements 2,3 and 4 are higher than that obtained in Fig. 11. And the twist of elements 1 (wing root) and 5 (wing tip) are closer to that obtained in Fig. 11. The same can be seen when the results of Figs. 29c and 13 are compared. The negative wing twist (down) is lower when there is no wing sweep.

And also, the Figs. 8 to 11 did not present flutter at 224.6m/s, for the three positions of the wing reference axis simulated. In Fig. 29b-d, the main difference is that the wing did not have sweep and the flutter occurred at the same airspeed of 224.6m/s. It means the wing sweep has one important effect on the aeroelastic stability.

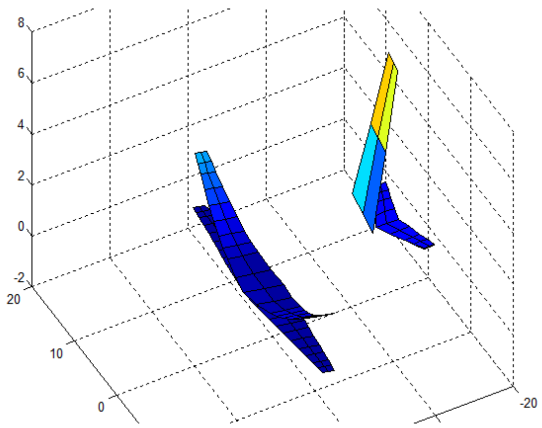

Fig. 28a. Airplane with zero wing sweep trimmed at 224.6m/s and at 10000 m, EA=0.00c

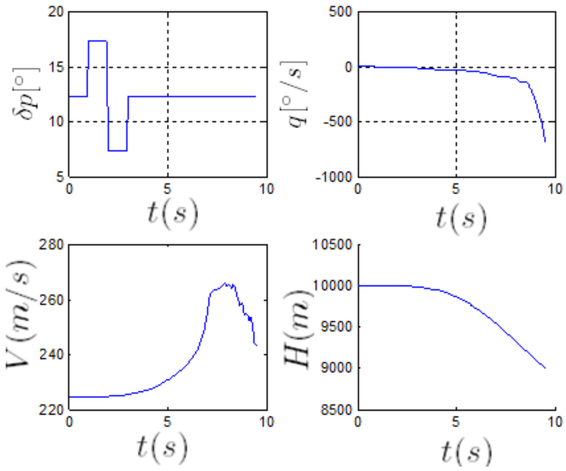

Fig. 28b. Airplane with zero wing sweep, response to elevator doublet, V=224.6m/s, EA=0.00c

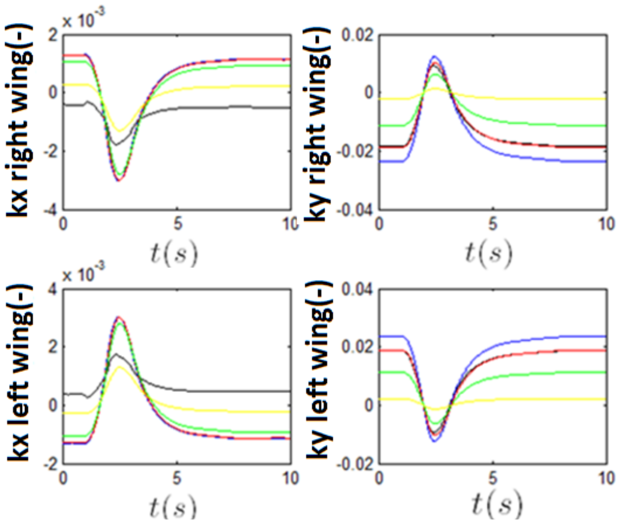

Fig. 28c. Airplane with zero wing sweep, response to elevator doublet, V=224.6m/s, EA=0.00c

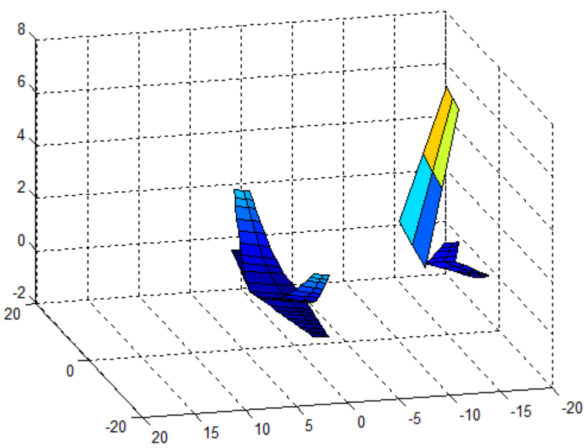

Fig. 29a. Airplane with zero wing sweep trimmed at 224.6m/s and at 10000 m, EA=-0.25c

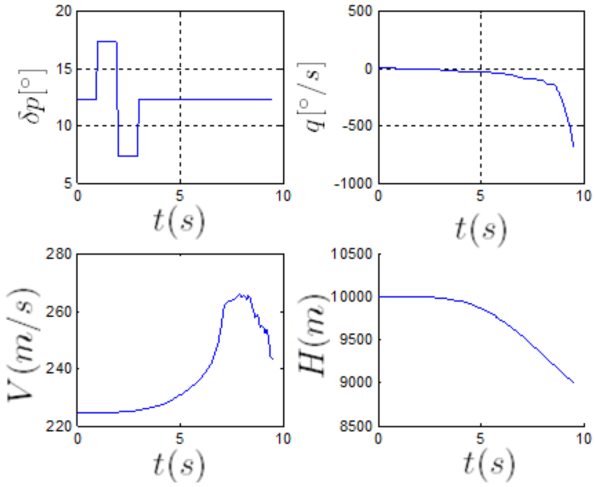

Fig. 29b. Airplane with zero wing sweep, response to elevator doublet, V=224.6m/s, EA=-0.25c

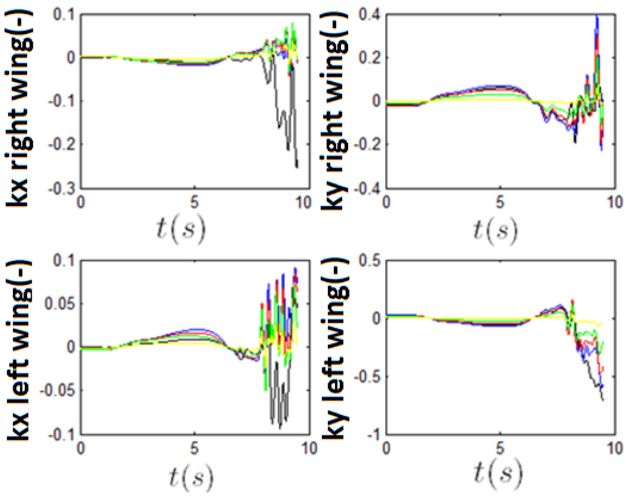

Fig. 29c. Airplane with zero wing sweep, response to elevator doublet, V=224.6m/s, EA=-0.25c

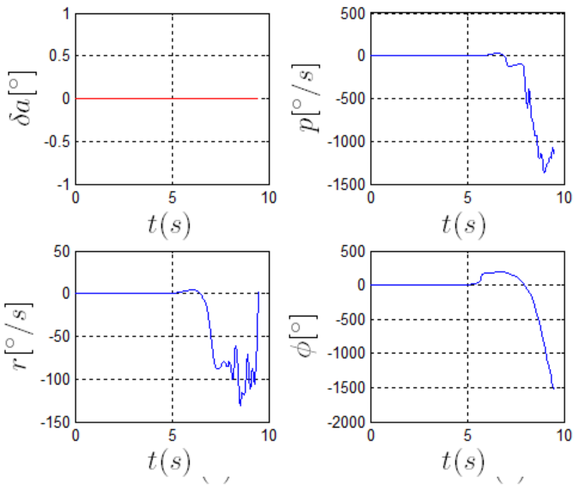

Fig. 29d. Airplane with zero wing sweep, response to elevator doublet, V=224.6m/s, EA=-0.25c

Fig. 29d presented elevated values of yaw and roll rates and roll angle during the flutter. Fig. 29c presented asymmetry on the bending and twist deformations. Both results are consistent and seem to indicate that the flutter occurred due to asymmetric modes. It should be noted that elevator deflection would not cause roll rates, even less with the amplitude presented on Fig. 29d. The roll rate with high amplitude was caused by asymmetrical modes. Fig. 29c shows that the structural torsion on left and right wings are significantly different. And the bending on the different sides are significantly different also. The model is capable to transmit the structural loads to the “rigid” aircraft. In order words, the formulation and model used allows the visualization of coupling between the flight and aeroelastic dynamics [38].

The results of this paper presented that the elastic axis / flexural axis position have strong effects on the aeroelastic stability and flight dynamics of very flexible airplanes.

6. CONCLUSIONS

This paper presented the analysis of influence of the elastic axis/ flexural axis positions on the flight dynamics and aeroelastic stability of one very flexible airplane, whose dynamics was modeled with the strain based formulation (NFNS_s methodology).

These new data presented here contribute to the better comprehension of couplings between flight and aeroelastic dynamics.

The time marching simulations performed, the detailed analysis made, the conclusions found and presented in the previous paragraphs were the contributions of this work. Other contribution was the use of NFNS_s to perform simulations and analysis of one very flexible transport category aircraft.

The limitation of this study is the use of the same stiffness matrices for all the cases analyzed. It is known that the elastic axis position influences the values of the stiffness matrix [21]. Other limitations are the facts of considering only quasi steady aerodynamics and not considering transonic effects.

In the analyses made, it was considered that the wing reference axis position described in Sousa [12], Su [19] corresponds to the local flexural axis position or is close to. The results presented here seem to validate the assumption made.

Despite the comments presented, the elastic axis and flexural axis positions are parameters that has influence not only on the aeroelastic dynamics, but also on the airplane flight dynamics of very flexible airplanes. And the effect of these parameters must be well understood and analyzed during the development of flexible airplanes.

The qualitative validation of the results obtained with the NFNS_s methodology is one stimulus to the use of this methodology to analyze the flight dynamics and aeroelasticity of very flexible airplanes.

COMPETING INTERESTS

Authors have declared that no competing interests exist.

REFERENCES

1. Nelson RC. Flight stability and automatic control. New York: Mc Graw Hill. 1989;284.
2. Schwithal J, Buch JP, Seehof C, Júnior MAA, Drewiacki D, Moreira FJO. Simulating Flexible Aircraft in a Full Motion Simulator -AIAA 2023-2318, AIAA Aviation 2023 Forum, San Diegom CA and Online; 2023. Available:https://doi.org/10.2514/6.2023-3318>, Accessed on April, 12th, 2024
3. Silvestre FJ. Modelagem da mecânica de vôo de aviões flexíveis e aplicações de controle. 116f. Thesis (Master in Aeronautical Engineering) – Technological Institute of Aeronautics, São José dos Campos; 2007.
4. Navaratna PDB, Pontillo A, Rezgui D, Lowenberg MH, Neild SA, Cooper JE. Numerical Investigations of Subscale Flexible High Aspect Ratio Aircraft on a Dynamic Wind Tunnel Rig. AIAA 2023-2559.AIAA SciTech Forum; 2023.\ Available:https://doi.org/10.2514/6.2023-1559>, Acessed on April 12th, 2023.
5. Shearer C. Coupled non linear and flight dynamics, aeroelasticity and control of very flexible aircraft. Dissertation (Doctorate in Aerospace Engineering) - University of Michigan, Ann Arbor. 2006;236.
6. Da Silva AL. Non-linear optimal model following control of flexible aircraft. Saarbrücken: LAP Lambert Academic. 2012;217.
7. Guimarães Neto AB. Dinâmica e controle de aeronaves flexíveis com modelagem

aerodinâmica pelo método doublet-lattice.. Disssertation (Graduation final work in Aeronautical Engineering) – Technological Institute of Aeronautics, São José dos Campos. 2008;179.

8. Pogorzielski G. Dinâmica de aviões flexiveis com modelagem aerodinâmica pela teoria das faixas não estacionária.. Tese (Mestrado em Engenharia Aeronáutica) - Instituto Tecnológico de Aeronáutica, São José dos Campos. 2010; 326.
9. Schmidt DK, Raney DL. Modeling and simulation of Flexible Flight Vehicles. AIAA Journal of Guidance, Control and Dynamics. 2001;24(3):539-546.
10. Silvestre FJ, Paglione P. Dynamics and Control of a Flexible Aircraft. AIAA Atmospheric Flight Mechanics Conference and Exhibit, Honolulu, Hawaii; 2008.
11. Waszak MR, Buttril CS, Schmidt DK. Modeling and model simplification of aeroelastic vehicles: an overview. Washington, DC: NASA. (NASA TM 107691); 1992.
12. Sousa MS. Modelagem, simulação e controle não linear de aviões muito flexíveis. Thesis (Doctorate in Aeronautical Engineering) – Technological Institute of Aeronautics, São José dos Campos. 2013; 389.
13. Meirovitch L, Tuzcu I. Unified theory for the dynamics and control of maneuvering flexible aircraft. AIAA Journal. 2004;42(4): 714-727.
14. Tuzcu I. Dynamics and control of flexible aircraft. Dissertation (Doctorate in Mechanical Engineering) –Virginia Polytechnique Institute and State University, Virginia. 2001;95.
15. Palacios R, Murua J, Cook R. Structural and aerodynamic models in the nonlinear flight dynamics of very flexible aircraft. AIAA Journal. 2010;48(11):2648-2659.
16. Brown EL. Integrated strain actuation in aircraft with highly flexible composite wings. Thesis (Doctorate in Mechanical Engineering) – Massachusetts Institute of Technology, Cambridge. 2003;205.
17. Palacios R, Cesnik CES. Structural models for flight dynamic analysis of very flexible aircraft. 50th AIAA/ASME/ASCE/AHS/ASC Structures, Structural Dynamics and Materials Conference and Exhibit, Palm Springs, California. AIAA Paper No. 2009-2403; 2009.
18. Ribeiro FLC. Dinâmica de vôo de aviões muito flexíveis. 158f. Thesis (Master in Aeronautical Engineering)–Technological Institute of Aeronautics, São José dos Campos; 2011.
19. Su W. Coupled non linear aeroelasticity and flight dynamics of fullly flexible aircraft. 266f.Dissertation (Doctorate in Aerospace Engineering) -University of Michigan, Ann Harbor; 2008.
20. Su W, Cesnik CES. Strain based geometrically nonlinear beam formulation for modeling very flexible aircraft. International Journal of Solids and Structures. 2010;48:2349-2360.
21. Palacios R, Cesnik CES. Dynamics of flexible aircraft: Coupled flight mechanics, aeroelasticity, and conrtrol (Cambridge Aerospace Series, Series Number 52) 1st Edition; 2023.
22. Cesnik CES, Brown EL. Modeling of high aspect ratio active flexiblewings for roll control. Proceedings of the 43rd AIAA/ASME/ASCE/AHS Structures, Structural Dynamics, and Materials Conferences, Denver, Colorado, AIAA Paper No. 2002-1719;2002.
23. Patil M, Hodges DH, Cesnik CES. Nonlinear aeroelasticity and flight dynamics of high altitute long endurance aircraft. AIAA Journal of Aircraft. 2001;38(01):88-94.
24. Raghavan B, Patil M. Flight dynamics of high aspect-ratio flying wings: Effect of large trim deformation. Journal of Aircraft. 2009;46(5).
25. Huo SH, Wang FS, Yuan Z, Yue ZF. Composite wing elastic axis for aeroelasticity optimization design. Aircraft Engineering and Aerospace Technology. 2013;85(1):10-15.
26. Baluch HA, Van Tooren M. Modified inertially coupled equations of motion for flexible aircraft with coupled equations. Journal of Aircraft. 2009;46(1):107-115.
27. Wright JR, Cooper JE. Introduction to aircraft aeroelasticity and loads. Washington, DC: AIAA Education Series. 2007;499.
28. Babcock JT. Aeroservoelastic design for closed-loop flight dynamics of a MAV. Doctorate dissertation. University of Florida; 2013.
29. Drela M. Integrated Simulation Model for Preliminary Aerodynamic, Structural, and Control-Law Design of Aircraft", AIAA 99-1394. 40th AIAA/ASME/ ASCE/AHS/ASC

Structures, Structural Dynamics, and Materials Conference and Exhibit; 1999.
30. Stodieck O, Cooper JE, Weaver PM. Interpretation of Bending/ Torsion Coupling for Swept. Nonhomogeneous Wings, Journal of Aircraft. 2016;53(4). DOI: 10.1364.C033186
31. Sousa MS, Paglione P, Silva RGA, Cardoso-Ribeiro FL, Cunha JR SS. Mathematical model of one flexible transport category aircraft. Aircraft Engineering and Aerospace Technology. 2017;89(3):384-396.
32. Goldstein H. Classical Mechanics. Addison-Wesley Publishing Company, Inc; 1980.
33. Aerospaceweb,. Wing twist and duhedralP; 2000. Available:https://aerospaceweb.org/question/dynamics/q0055.shtml>. Acessed on April, 9th, 2024.
34. Sofla AYN, Meguid SA, Tan KT, Yeo WK. Shape morphing of aircraft wing: status and challenges. Materials and Design. 2010;31(3):1284-1292.
35. Sharma U, Effects of Airfoil Geometry and Mechanical Charactheristics on the Onset of Flutter; 2004. Available:http://www.its.caltech.edu/~mason/research/woody.pdf>. Access on June, 23rd, 2013
36. Quora. What's the airliner with the largest wing flex?; 2016 Available:https://www.quora.com/Whats-the-airliner-with-the-largest-wing-flex>.Accessed on April, 12th, 2024
37. Bisplinhoff RL, Ashley H. Principles of Aeroelasticity. Dover Publications, Inc; 2013.
38. Coccon MN, Menegozzo M, Galvanetto U. New methodologies in reliability-based design optimization for aerospace structures. 11th World Congress on Computational Mechanics (WCCM XI), Barcelona, Spain; 2014.

Peer-review history:
The peer review history for this paper can be accessed here:
https://www.sdiarticle5.com/review-history/116101